ISSN 2186-6570

Homodyne measurement with angle ϕ rotation and its application to the detection of squeezed state signal

Kentaro Kato

Quantum Communication Research Center,
Quantum ICT Research Institute, Tamagawa University
6-1-1 Tamagawa-gakuen, Machida, Tokyo 194-8610, Japan

Tamagawa University Quantum ICT Research Institute Bulletin, Vol.12, No.1, 15-27, 2022

Homodyne measurement with angle ϕ rotation and its application to the detection of squeezed state signal

Kentaro Kato
Quantum Communication Research Center,
Quantum ICT Research Institute, Tamagawa University
6-1-1 Tamagawa-gakuen, Machida, Tokyo 194-8610, Japan
E-mail: kkatop@lab.tamagawa.ac.jp

***Abstract*—Homodyne measurement with angle ϕ rotation is considered in the scenario of quantum communications. First, some essential characteristics of the homodyne measurement with angle ϕ rotation are investigated in the cases of coherent and squeezed states. Second, the homodyne receiver with angle ϕ rotation is applied to the signal detection problem of binary squeezed state signal.**

I. Introduction

Homodyne measurement is one of the effective techniques to detect light. The references [1], [2], [3], [4], [5], [6] are early discussions on the quantum mechanical treatment and the analysis of homodyne measurement in the scenario of optical communications and precision measurement of light. In quantum state tomography ([7], [8], [9], [10], etc.), homodyne measurement is essential in realizing it.

The squeezed state (once called the two-photon coherent state) is one of the fundamental states of light ([11], [12], [13], [14], etc.). From the viewpoint of quantum information science, the squeezed states possess several potential applications. For example, the reference [11] pointed out that the transmission source and the ideal amplifier for optical communications are valuable applications. Early discussions on these issues by the first generation of quantum information scientists can be found in the references [2], [3], [4], [13], [15], [16]. These issues have recently returned to the spotlight, and more advanced research reports have emerged. For example, the references [17], [18] discuss the basic properties of the squeezed state-based quantum communication systems with phase-shift keying signal format. In addition, the references [19], [20] report some propagation characteristics of the squeezed light in fog toward future applications such as free-space quantum communications and quantum-enhanced target detection.

This paper discusses homodyne measurement with angle ϕ rotation and how to apply it for detecting squeezed state signals in the scenario of quantum communications. Suppose that M-ary phase-shift keying squeezed state signals are prepared, and the signals are divided into $M/2$ pairs, each consisting of the signals apart from π radian. The problem treated in this paper is the discrimination of the two signals in a pair by the homodyne receiver that consists of a homodyne measurement scheme and appropriate decision-making rule for signal detection. At that time, the measurement angle in the homodyne receiver must be adjusted according to the target pair to avoid performance degradation due to a mismatch of the signaling phase and measurement angle. Therefore, we first investigate some essential characteristics of the homodyne measurement with angle ϕ rotation in the cases of coherent and squeezed states. After that, the homodyne receiver with angle ϕ is applied to the detection problem of binary squeezed state signal.

II. Homodyne measurement with angle ϕ rotation

A. Coherent state case

For a single mode of the field with the annihilation operator $\hat{a}$ and the creation operator $\hat{a}^\dagger$, define the observables $\hat{X}_{\rm c} \equiv (\hat{a}^\dagger + \hat{a})/2$ and $\hat{X}_{\rm s} \equiv \jmath(\hat{a}^\dagger - \hat{a})/2$, where $\jmath = \sqrt{-1}$. These observables obey the relation $[\hat{X}_{\rm c}, \hat{X}_{\rm s}] = \jmath/2$. The eigenvectors $|x_{\rm c}\rangle$ of $\hat{X}_{\rm c}$ (*i.e.*, $\hat{X}_{\rm c}|x_{\rm c}\rangle = x_{\rm c}|x_{\rm c}\rangle$) form an orthonormal basis $\{|x_{\rm c}\rangle\}$ of the Hilbert space corresponding to the mode under consideration. Similarly, $\{|x_{\rm s}\rangle\}$ is an orthonormal basis. The $x_{\rm c}$- and $x_{\rm s}$-representations of the coherent state $|\alpha'\rangle_{\rm coh}$ of complex amplitude α' are respectively given as follows (p.127 and p.255 of [1]):

$$\langle x_{\rm c}|\alpha'\rangle_{\rm coh} = \left(\frac{2}{\pi}\right)^{1/4} \exp[-x_{\rm c}^2 + 2\alpha' x_{\rm c} - \frac{1}{2}|\alpha'|^2 - \frac{1}{2}\alpha'^2], \quad (1)$$

$$\langle x_{\rm s}|\alpha'\rangle_{\rm coh} = \left(\frac{2}{\pi}\right)^{1/4} \exp[-x_{\rm s}^2 - 2\jmath\alpha' x_{\rm s} - \frac{1}{2}|\alpha'|^2 + \frac{1}{2}\alpha'^2]. \quad (2)$$

Therefore, the probability density function (PDF) of measurement outcome $x_{\rm c}$ by the projection-valued measure

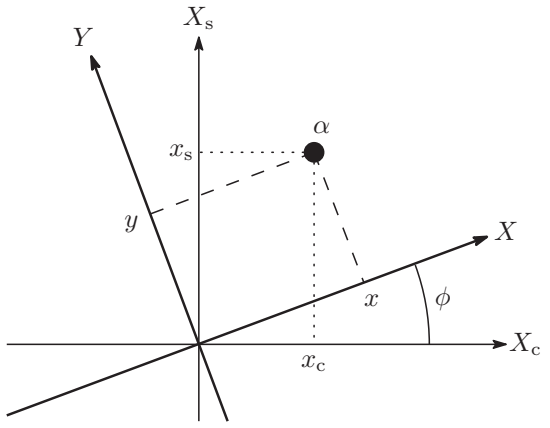

Fig. 1. Coordinates (X_c, X_s) and (X, Y)

$\{|x_c\rangle\langle x_c|\}$ and that of x_s by $\{|x_s\rangle\langle x_s|\}$ are respectively given [1] as

$$p(x_c|\alpha') = \sqrt{\frac{2}{\pi}}\exp[-2\left(x_c - \frac{\alpha'^* + \alpha'}{2}\right)^2], \quad (3)$$

$$p(x_s|\alpha') = \sqrt{\frac{2}{\pi}}\exp[-2\left(x_s - \jmath\frac{\alpha'^* - \alpha'}{2}\right)^2]. \quad (4)$$

Next, define the observable $\hat{X}_\phi \equiv (\hat{a}^\dagger \mathrm{e}^{\jmath\phi} + \hat{a}\mathrm{e}^{-\jmath\phi})/2$, $\hat{X} \equiv \hat{X}_\phi$ and $\hat{Y} \equiv \hat{X}_{\phi+\pi/2}$, where ϕ is real. The commutator of $\hat{X}$ and $\hat{Y}$ is $[\hat{X}, \hat{Y}] = \jmath/2$. The geometrical relation of the two coordinates (X_c, X_s) and (X, Y) is illustrated in Fig. 1.

Let $|x\rangle$ and $|y\rangle$ denote eigenstates of $\hat{X}$ and $\hat{Y}$, respectively. A simple way to find the x- and y-representations of coherent state $|\alpha\rangle_{\mathrm{coh}}$ is to use the rotation operator $\hat{R}(\phi) = \exp[-\jmath\phi\hat{a}^\dagger\hat{a}]$. Since $\hat{R}(\phi)\hat{X}\hat{R}^\dagger(\phi) = \hat{X}_c$, the eigen equation $\hat{X}(\hat{R}^\dagger(\phi)|x_c\rangle) = x_c(\hat{R}^\dagger(\phi)|x_c\rangle)$ holds. Therefore,

$$\begin{aligned}\langle x|\alpha\rangle_{\mathrm{coh}} &= \langle x_c|\hat{R}(\phi)\hat{D}(\alpha)|0\rangle \\ &= \langle x_c|\hat{D}(\mathrm{e}^{-\jmath\phi}\alpha)\hat{R}^\dagger(\phi)|0\rangle \\ &= \langle x_c|\hat{D}(\mathrm{e}^{-\jmath\phi}\alpha)|0\rangle \\ &= \langle x_c|\mathrm{e}^{-\jmath\phi}\alpha\rangle_{\mathrm{coh}}, \end{aligned} \quad (5)$$

where $\hat{D}(\alpha') = \exp[\alpha'\hat{a}^\dagger - \alpha'^*\hat{a}]$ is the displacement operator with complex amplitude $\alpha' \in \mathbb{C}$. Similarly,

$$\langle y|\alpha\rangle_{\mathrm{coh}} = \langle x_s|\alpha\mathrm{e}^{-\jmath\phi}\rangle_{\mathrm{coh}} \quad (6)$$

from $\hat{R}(\phi)\hat{Y}\hat{R}^\dagger(\phi) = \hat{X}_s$. Therefore,

$$\langle x|\alpha\rangle_{\mathrm{coh}} = \left(\frac{2}{\pi}\right)^{1/4}\exp[-x^2 + 2\alpha\mathrm{e}^{-\jmath\phi}x - \frac{1}{2}|\alpha|^2 - \frac{1}{2}\alpha^2\mathrm{e}^{-2\jmath\phi}], \quad (7)$$

$$\langle y|\alpha\rangle_{\mathrm{coh}} = \left(\frac{2}{\pi}\right)^{1/4}\exp[-y^2 - 2\jmath\alpha\mathrm{e}^{-\jmath\phi}y - \frac{1}{2}|\alpha|^2 + \frac{1}{2}\alpha^2\mathrm{e}^{-2\jmath\phi}]. \quad (8)$$

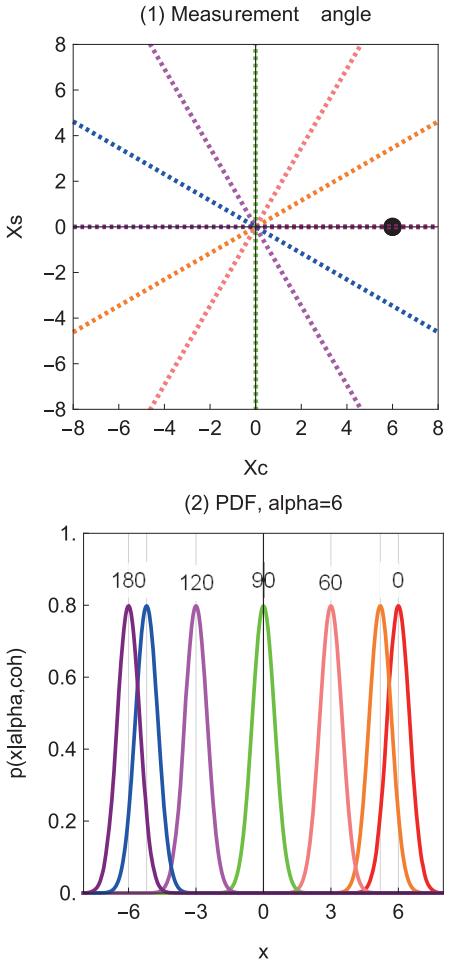

Fig. 2. Homodyne of coherent state. (1) measurement angle. (2) probability density function. $\phi = 0°$:red, $30°$:orange, $60°$:pink, $90°$:green, $120°$:magenta, $150°$:blue, $180°$:purple. Dot in (1) stands for the complex amplitude $\alpha = 6$.

Note that Eqs. (7) and (8) can be derived directly from the following differential equations:

$$\frac{\partial}{\partial x}\langle x|\alpha\rangle_{\mathrm{coh}} = 2(\alpha\mathrm{e}^{-\jmath\phi} - x)\langle x|\alpha\rangle_{\mathrm{coh}}, \quad (9)$$

$$\frac{\partial}{\partial y}\langle y|\alpha\rangle_{\mathrm{coh}} = 2(\alpha\mathrm{e}^{-\jmath(\phi+\frac{\pi}{2})} - y)\langle y|\alpha\rangle_{\mathrm{coh}}, \quad (10)$$

which are established by evaluating $\langle x|\hat{a}|\alpha\rangle_{\mathrm{coh}}$ and $\langle y|\hat{a}|\alpha\rangle_{\mathrm{coh}}$, respectively.

From the x-representation $\langle x|\alpha\rangle_{\mathrm{coh}}$, the PDF of outcome x by the projection-valued measure $\{|x\rangle\langle x|\}$ is

$$\begin{aligned} p(x|\alpha) &= |\langle x|\alpha\rangle_{\mathrm{coh}}|^2 \\ &= \sqrt{\frac{2}{\pi}}\exp[-2\left(x - \bar{X}_{\mathrm{coh}}\right)^2], \end{aligned} \quad (11)$$

where the mean and varicance are

$$\bar{X}_{\mathrm{coh}} = \frac{\mathrm{e}^{\jmath\phi}\alpha^* + \mathrm{e}^{-\jmath\phi}\alpha}{2}, \quad \sigma^2_{X,\mathrm{one,coh}} = \frac{1}{4}. \quad (12)$$

The PDF of y by $\{|y\rangle\langle y|\}$ is

$$p(y|\alpha) = |\langle y|\alpha\rangle_{\rm coh}|^2 = \sqrt{\frac{2}{\pi}}\exp[-2\left(y-\bar{Y}_{\rm coh}\right)^2], \quad (13)$$

where

$$\bar{Y}_{\rm coh} = \jmath\frac{{\rm e}^{\jmath\phi}\alpha^* - {\rm e}^{-\jmath\phi}\alpha}{2}, \quad \sigma^2_{Y,{\rm one,coh}} = \frac{1}{4}. \quad (14)$$

The means $\bar{X}_{\rm coh}$ and $\bar{Y}_{\rm coh}$ depend on the measurement angle ϕ, while the variances $\sigma^2_{X,{\rm one,coh}}$ and $\sigma^2_{Y,{\rm one,coh}}$ are independent from ϕ. Fig. 2 shows $p(x|\alpha)$ for some measurement angles at $\alpha = 6$.

For the coherent state case, Robertson's inequality [21] is satisfied with minimal uncertainty, independent from ϕ:

$$\sigma^2_{X,{\rm one,coh}}\sigma^2_{Y,{\rm one,coh}} = \frac{1}{16} = \frac{1}{4}\Big|[\hat{X},\hat{Y}]\Big|^2. \quad (15)$$

B. Squeezed state case

Let $|\beta;\mu,\nu\rangle$ denote a squeezed state having complex parameters β, μ, and ν, where $|\mu|^2 - |\nu|^2 = 1$ (Basic properties of the squeezed states are summarized according to the reference [11] in Appendix *A*).

The following differential equations are obtained by evaluating $\langle x|\hat{b}|\beta;\mu,\nu\rangle$ and $\langle y|\hat{b}|\beta;\mu,\nu\rangle$:

$$\Big(\beta - \Lambda_+[\phi]x\Big)\langle x|\beta;\mu,\nu\rangle = \frac{1}{2}\Lambda_-[\phi]\frac{\partial}{\partial x}\langle x|\beta;\mu,\nu\rangle, \quad (16)$$

$$\Big(\beta - \Lambda_+[\phi+\frac{\pi}{2}]y\Big)\langle y|\beta;\mu,\nu\rangle = \frac{1}{2}\Lambda_-[\phi+\frac{\pi}{2}]\frac{\partial}{\partial y}\langle y|\beta;\mu,\nu\rangle, \quad (17)$$

where

$$\Lambda_-[\phi] = \mu{\rm e}^{\jmath\phi} - \nu{\rm e}^{-\jmath\phi}, \quad (18)$$

$$\Lambda_+[\phi] = \mu{\rm e}^{\jmath\phi} + \nu{\rm e}^{-\jmath\phi} \quad (19)$$

(See also Appendix *E*). Solving the differential equations, the x- and y-representations of the squeezed state $|\beta;\mu,\nu\rangle$ are respectively given as

$$\langle x|\beta;\mu,\nu\rangle = \left(\frac{2}{\pi}\right)^{1/4}\left(\frac{{\rm e}^{\jmath\phi}}{\Lambda_-[\phi]}\right)^{1/2} \times\exp\Big[-\frac{\Lambda_+[\phi]}{\Lambda_-[\phi]}x^2 + \frac{2}{\Lambda_-[\phi]}\beta x - \frac{1}{2}|\beta|^2 - \frac{1}{2}\cdot\frac{\Lambda^*_-[\phi]}{\Lambda_-[\phi]}\beta^2\Big], \quad (20)$$

$$\langle y|\beta;\mu,\nu\rangle = \left(\frac{2}{\pi}\right)^{1/4}\left(\frac{{\rm e}^{\jmath\phi}}{\Lambda_+[\phi]}\right)^{1/2} \times\exp\Big[-\frac{\Lambda_-[\phi]}{\Lambda_+[\phi]}y^2 - \jmath\frac{2}{\Lambda_+[\phi]}\beta y - \frac{1}{2}|\beta|^2 + \frac{1}{2}\cdot\frac{\Lambda^*_+[\phi]}{\Lambda_+[\phi]}\beta^2\Big]. \quad (21)$$

The PDF of outcome x by the projection-valued measure $\{|x\rangle\langle x|\}$ for the squeezed state $|\beta;\mu,\nu\rangle$ is

$$p(x|\beta;\mu,\nu) = \frac{1}{\sqrt{2\pi\sigma^2_{X,{\rm one,sq}}}}\exp[-\frac{(x-\bar{X}_{\rm sq})^2}{2\sigma^2_{X,{\rm one,sq}}}], \quad (22)$$

where the mean and variance are

$$\bar{X}_{\rm sq} = \frac{\Lambda_-[\phi]\beta^* + \Lambda^*_-[\phi]\beta}{2}, \quad (23)$$

$$\sigma^2_{X,{\rm one,sq}} = \frac{1}{4}\big|\Lambda_-[\phi]\big|^2. \quad (24)$$

Similarly, the PDF of y by $\{|y\rangle\langle y|\}$ for $|\beta;\mu,\nu\rangle$ is

$$p(y|\beta;\mu,\nu) = \frac{1}{\sqrt{2\pi\sigma^2_{Y,{\rm one,sq}}}}\exp[-\frac{(y-\bar{Y}_{\rm sq})^2}{2\sigma^2_{Y,{\rm one,sq}}}], \quad (25)$$

where

$$\bar{Y}_{\rm sq} = \jmath\frac{\Lambda_+[\phi]\beta^* - \Lambda^*_+[\phi]\beta}{2}, \quad (26)$$

$$\sigma^2_{Y,{\rm one,sq}} = \frac{1}{4}\big|\Lambda_+[\phi]\big|^2. \quad (27)$$

All of the statistics (23), (24), (26), and (27), depends on measurement angle ϕ in the squeezed state case, while only the means depend on in the coherent state case.

Here, let us evaluate Robertson's inequality. If the state parameters μ and ν and the measurement angle ϕ satisfy the relation $\mu{\rm e}^{\jmath\phi} = c\nu{\rm e}^{-\jmath\phi}$ with a real number c, the condition $|\mu|^2 - |\nu|^2 = 1$ is replaced to the conditions $(c^2-1)|\nu|^2 = 1$ and $|c| \geq 1$. Once $\mu{\rm e}^{\jmath\phi} = c\nu{\rm e}^{-\jmath\phi}$ holds for a real number c, then $\mu{\rm e}^{\jmath(\phi+m\pi/2)} = (-1)^m c\nu{\rm e}^{-\jmath(\phi+m\pi/2)}$ for an integer m. Even in this case, $(c^2-1)|\nu|^2 = 1$ still holds. Under these conditions, the equality of Robertson's inequality is established:

$$\sigma^2_{X,{\rm one,sq}}\sigma^2_{Y,{\rm one,sq}} = \frac{1}{16}\big|\Lambda_-[\phi]\big|^2\big|\Lambda_+[\phi]\big|^2 = \frac{1}{16}\big|\Lambda_-[\phi+m\frac{\pi}{2}]\big|^2\big|\Lambda_+[\phi+m\frac{\pi}{2}]\big|^2 = \frac{1}{16}(c^2-1)^2|\nu|^4 = \frac{1}{16} = \frac{1}{4}\big|[\hat{X},\hat{Y}]\big|^2. \quad (28)$$

The variances are

$$\sigma^2_{X,{\rm one,sq}} = \frac{1}{4}\cdot\frac{c-1}{c+1}, \quad (29)$$

$$\sigma^2_{Y,{\rm one,sq}} = \frac{1}{4}\cdot\frac{c+1}{c-1}. \quad (30)$$

If $c > 1$, then $\sigma^2_{X,{\rm one,sq}} < \sigma^2_{Y,{\rm one,sq}}$. Conversely, if $c < -1$, then $\sigma^2_{Y,{\rm one,sq}} < \sigma^2_{X,{\rm one,sq}}$. Now, suppose the relation $\mu{\rm e}^{\jmath\phi} = c\nu{\rm e}^{-\jmath\phi}$ holds for some $c > 1$ at measurement angle ϕ. Take the measurement angle $\phi + m\pi/2 + \pi/4$,

$$\sigma^2_{X,{\rm one,sq}} = \frac{1}{4}\cdot\frac{c^2+1}{c^2-1} = \sigma^2_{Y,{\rm one,sq}}. \quad (31)$$

To illustrate the property of the uncertainty product $\sigma^2_{X,{\rm one,sq}}\sigma^2_{Y,{\rm one,sq}}$ concretely, assume that $\mu = \cosh r$ and

$\nu = \mathrm{e}^{2\jmath\theta_{\rm sq}} \sinh r$, where $r > 0$ and $-\pi/2 < \theta_{\rm sq} \le \pi/2$. Under this assumption,

$$\begin{aligned}\sigma^2_{X,\rm one,sq}\sigma^2_{Y,\rm one,sq} &= \frac{1}{16}\left|\Lambda_-[\phi]\right|^2\left|\Lambda_+[\phi]\right|^2 \\ &= \frac{1}{16}\big(\cosh^4 r + \sinh^4 r \\ &\quad -2\cos[4(\theta_{\rm sq}-\phi)]\cosh^2 r \sinh^2 r\big). \end{aligned} \quad (32)$$

A typical behavior of the product of variances is shown in Fig. 3. If $\theta_{\rm sq} - \phi = m\pi/2$ for integer m, Robertson's inequality is satisfied with minimum uncertainty:

$$\sigma^2_{X,\rm one,sq}\sigma^2_{Y,\rm one,sq}\big|_{\theta_{\rm sq}-\phi=m\pi/2} = \frac{1}{16} = \frac{1}{4}\left|[\hat{X},\hat{Y}]\right|^2. \quad (33)$$

Further, the ratio of the variances is calculated as

$$\begin{aligned}\frac{\sigma^2_{Y,\rm one,sq}}{\sigma^2_{X,\rm one,sq}} &= \Big(\cosh^4 r + \sinh^4 r \\ &\quad -2\cos[4(\theta_{\rm sq}-\phi)]\cosh^2 r \sinh^2 r\Big) \\ &\quad /\Big(\cosh[2r] \\ &\quad -\cos[2(\theta_{\rm sq}-\phi)]\sinh[2r]\Big)^2. \end{aligned} \quad (34)$$

This ratio is illustrated in Fig. 4, and one can observe that

$$\sigma^2_{X,\rm one,sq} = \frac{1}{4}\mathrm{e}^{-2r} < \sigma^2_{Y,\rm one,sq} = \frac{1}{4}\mathrm{e}^{2r} \quad (35)$$

for $\theta_{\rm sq} - \phi = 0, \pm\pi$,

$$\sigma^2_{X,\rm one,sq} = \frac{1}{4}\mathrm{e}^{2r} > \sigma^2_{Y,\rm one,sq} = \frac{1}{4}\mathrm{e}^{-2r} \quad (36)$$

for $\theta_{\rm sq} - \phi = \pm\pi/2$, and

$$\sigma^2_{X,\rm one,sq} = \sigma^2_{Y,\rm one,sq} = \frac{1}{4}\cosh[2r] \quad (37)$$

for $\theta_{\rm sq} - \phi = \pm\pi/4, \pm 3\pi/4$.

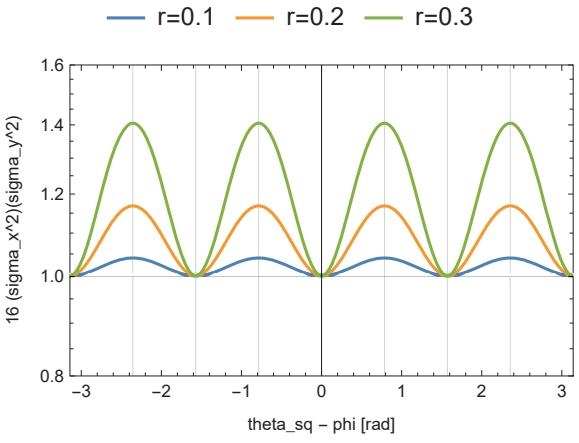

Fig. 3. $16\sigma^2_{X,\rm one,sq}\sigma^2_{Y,\rm one,sq}$ vs. $\theta_{\rm sq} - \phi$ [rad] when $\mu = \cosh r$ and $\nu = \mathrm{e}^{2\jmath\theta_{\rm sq}}\sinh r$.

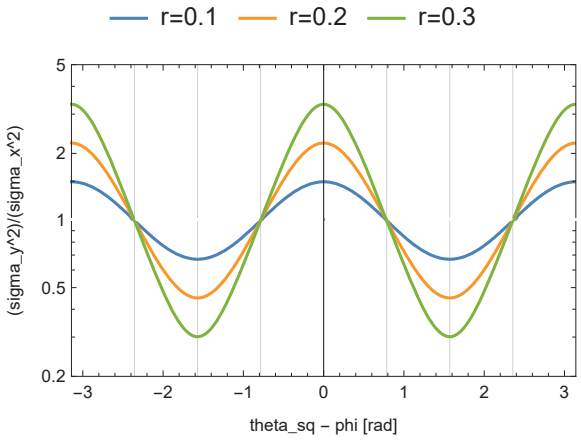

Fig. 4. $\sigma^2_{Y,\rm one,sq}/\sigma^2_{X,\rm one,sq}$ vs. $\theta_{\rm sq} - \phi$ [rad] when $\mu = \cosh r$ and $\nu = \mathrm{e}^{2\jmath\theta_{\rm sq}}\sinh r$.

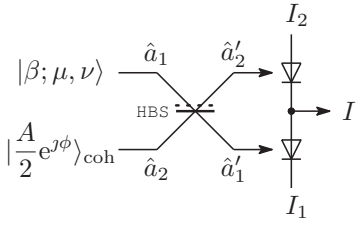

Fig. 5. Balanced homodyne measurement with angle ϕ

Fig. 5 shows a physical set-up of $\{|x\rangle\langle x|\}$, which is known as the balanced homodyne measurement [5]. In this scheme, the input-output relation of the half beam splitter (HBS) is assumed to be

$$\hat{a}_1' = (\hat{a}_1 - \hat{a}_2)/\sqrt{2}, \quad (38)$$
$$\hat{a}_2' = (\hat{a}_1 + \hat{a}_2)/\sqrt{2}. \quad (39)$$

The photo current I_1 is proportional to the photon number $\hat{a}_1'^\dagger\hat{a}_1'$. Hence we let $\hat{I}_1 = \hat{a}_1'^\dagger\hat{a}_1'$, assuming the quantum efficiency is unity. With the same reason, $\hat{I}_2 = \hat{a}_2'^\dagger\hat{a}_2'$. Therefore,

$$\hat{I} = \hat{I}_2 - \hat{I}_1 = \hat{a}_1^\dagger\hat{a}_2 + \hat{a}_1\hat{a}_2^\dagger \quad (40)$$

and

$$\begin{aligned}\hat{I}^2 &= \hat{a}_1^{\dagger 2}\hat{a}_2^2 + \hat{a}_1^2\hat{a}_2^{\dagger 2} \\ &\quad +\hat{a}_1^\dagger\hat{a}_1 + 2\hat{a}_1^\dagger\hat{a}_1\hat{a}_2^\dagger\hat{a}_2 + \hat{a}_2^\dagger\hat{a}_2. \end{aligned} \quad (41)$$

When the input state of port 1 is the squeezed state $|\psi_1\rangle = |\beta;\mu,\nu\rangle$ and the local oscillator at port 2 is $|\psi_2\rangle = |(A/2)\mathrm{e}^{\jmath\phi}\rangle_{\rm coh}$ with $A > 0$, then

$$\begin{aligned}\bar{I} &= \langle\hat{I}\rangle \\ &= A \times \frac{\Lambda_-[\phi]\beta^* + \Lambda_-^*[\phi]\beta}{2}, \end{aligned} \quad (42)$$

$$\begin{aligned}\Sigma_I^2 &= \langle\hat{I}^2\rangle - \langle\hat{I}\rangle^2 \\ &= A^2 \times \frac{1}{4}\left|\Lambda_-[\phi]\right|^2 + \bar{n}_1 \\ &\approx A^2 \times \frac{1}{4}\left|\Lambda_-[\phi]\right|^2, \end{aligned} \quad (43)$$

where $\bar{n}_1 = |\mu^*\beta - \nu\beta^*|^2 + |\nu|^2$ and where the approximation holds for sufficiently large A. Re-scaling these statistics with A, $\bar{I} \to \bar{X}_{\rm sq}$ and $\Sigma_I^2 \to \sigma^2_{X,{\rm one,sq}}$. Thus, the balanced homodyne captures the mean $\bar{X}_{\rm sq}$ and variance $\sigma^2_{X,{\rm one,sq}}$ for the observable $\hat{X}$ when the oscillator phase is ϕ rad.

When the local oscillator light is changed to $|\psi_2\rangle = |(A/2)\mathrm{e}^{\jmath(\phi+\pi/2)}\rangle_{\rm coh}$, the average photo current and its variance are given as

$$\bar{I} = A \times \jmath\frac{\Lambda_+[\phi]\beta^* - \Lambda_+^*[\phi]\beta}{2}, \tag{44}$$

$$\Sigma_I^2 \approx A^2 \times \frac{1}{4}\big|\Lambda_+[\phi]\big|^2, \tag{45}$$

for $A \gg 1$, where these are obtained by replacing ϕ to $\phi + \pi/2$ in Eqs. (42) and (43) (Appendix *E*). Hence $\bar{I} \to \bar{Y}_{\rm sq}$ and $\Sigma_I^2 \to \sigma^2_{Y,{\rm one,sq}}$ by rescaling. Thus, the local oscillator phase $\phi + \pi/2$ provides the mean and variance of the observable $\hat{Y}$.

III. Homodyne measurement for two componets

The standard homodyne scheme for simultaneous detection of two non-commutative components measures $\hat{X}_{\rm c}$ and $\hat{X}_{\rm s}$ simultaneously, and it can be associated with $\{|\alpha\rangle_{\rm coh}\langle\alpha|/\pi : \alpha \in \mathbb{C}\}$, a positive operator-valued measure (POVM).

In this section, a simultaneous detection scheme of non-commutative components $\hat{X}$ and $\hat{Y}$ by homodyne measurement with angle ϕ rotation is considered. Since

$$\hat{a} = \hat{X}_{\rm c} + \jmath\hat{X}_{\rm s} = \mathrm{e}^{\jmath\phi}\Big(\hat{X} + \jmath\hat{Y}\Big),$$

the main task in the following analysis is just a coordinate change from $(X_{\rm c}, X_{\rm s})$ to (X, Y) by angle ϕ rotation. In other words, it means the corresponding POVM for the simultaneous detection of $\hat{X}$ and $\hat{Y}$ does not change; the POVM is $\{|\alpha\rangle_{\rm coh}\langle\alpha|/\pi : \alpha \in \mathbb{C}\}$. Therefore, the PDF of outcome (x, y) can be derived from the coordinate change. It is given by

$$\begin{aligned} &p(x,y|\beta;\mu,\nu) \\ &= \frac{1}{2\pi\sigma_{X,{\rm two,sq}}\sigma_{Y,{\rm two,sq}}\sqrt{1-\zeta_{XY}^2}} \\ &\quad\times\exp\Big[-\frac{1}{2(1-\zeta_{XY}^2)} \\ &\qquad\times\Big\{\frac{(x-\bar{X}_{\rm sq})^2}{\sigma^2_{X,{\rm two,sq}}} + \frac{(y-\bar{Y}_{\rm sq})^2}{\sigma^2_{Y,{\rm two,sq}}} \\ &\qquad -2\zeta_{XY}\frac{(x-\bar{X}_{\rm sq})(y-\bar{Y}_{\rm sq})}{\sigma_{X,{\rm two,sq}}\sigma_{Y,{\rm two,sq}}}\Big\}\Big], \end{aligned} \tag{46}$$

where

$$\bar{X}_{\rm sq} = \frac{\Lambda_-[\phi]\beta^* + \Lambda_-^*[\phi]\beta}{2}, \tag{47}$$

$$\sigma^2_{X,{\rm two,sq}} = \frac{1}{4}\Big(\big|\Lambda_-[\phi]\big|^2 + 1\Big), \tag{48}$$

$$\bar{Y}_{\rm sq} = \jmath\frac{\Lambda_+[\phi]\beta^* - \Lambda_+^*[\phi]\beta}{2}, \tag{49}$$

$$\sigma^2_{Y,{\rm two,sq}} = \frac{1}{4}\Big(\big|\Lambda_+[\phi]\big|^2 + 1\Big), \tag{50}$$

$$\zeta_{XY} = \jmath\frac{\Lambda_-^*[\phi]\Lambda_+[\phi] - \Lambda_-[\phi]\Lambda_+^*[\phi]}{2\sqrt{\Big(\big|\Lambda_-[\phi]\big|^2+1\Big)\Big(\big|\Lambda_+[\phi]\big|^2+1\Big)}}. \tag{51}$$

This can be arranged to the following form by means of the covariant matrix:

$$\begin{aligned} &p(x,y|\beta;\mu,\nu) \\ &= \frac{1}{2\pi\sqrt{\det(\mathbf{K})}}\exp[-\frac{1}{2}(\mathbf{x}-\mathbf{m})^t\mathbf{K}^{-1}(\mathbf{x}-\mathbf{m})], \end{aligned} \tag{52}$$

where $\mathbf{x} = [x, y]^t$, $\mathbf{m} = [\bar{X}_{\rm sq}, \bar{Y}_{\rm sq}]^t$ and

$$\mathbf{K} = \begin{bmatrix} K_{11} & K_{12} \\ K_{21} & K_{22} \end{bmatrix}, \tag{53}$$

$$\det(\mathbf{K}) = K_{11}K_{22} - K_{12}K_{21}, \tag{54}$$

$$\mathbf{K}^{-1} = \frac{1}{\det(\mathbf{K})}\begin{bmatrix} K_{22} & -K_{21} \\ -K_{12} & K_{11} \end{bmatrix}, \tag{55}$$

$$K_{11} = \sigma^2_{X,{\rm two,sq}}, \tag{56}$$

$$\begin{aligned} K_{12} &= \zeta_{XY}\times\sigma_{X,{\rm two,sq}}\times\sigma_{Y,{\rm two,sq}} \\ &= \jmath\frac{1}{8}\big(\Lambda_-^*[\phi]\Lambda_+[\phi] - \Lambda_-[\phi]\Lambda_+^*[\phi]\big) \\ &= K_{21}, \end{aligned} \tag{57}$$

$$K_{22} = \sigma^2_{Y,{\rm two,sq}}. \tag{58}$$

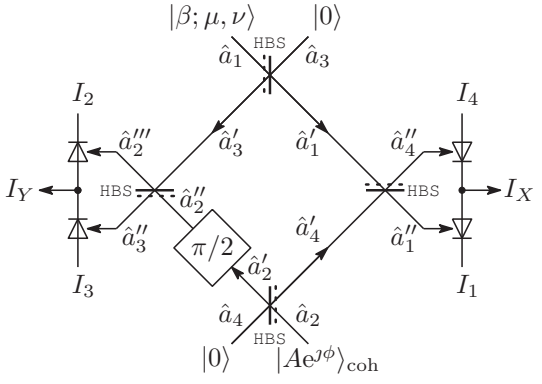

Fig. 6. homodyne with angle ϕ for two-component detection

Fig. 6 shows a physical set-up of the eight-port homodyne measurement. The input-output relation of the half

beam splitters is assumed as follows (See also [22]):

$$\hat{a}'_1 = \frac{1}{\sqrt{2}}(\hat{a}_1 - \hat{a}_3), \qquad \hat{a}'_3 = \frac{1}{\sqrt{2}}(\hat{a}_1 + \hat{a}_3), \quad (59)$$

$$\hat{a}'_2 = \frac{1}{\sqrt{2}}(\hat{a}_2 - \hat{a}_4), \qquad \hat{a}'_4 = \frac{1}{\sqrt{2}}(\hat{a}_2 + \hat{a}_4), \quad (60)$$

$$\hat{a}''_1 = \frac{1}{\sqrt{2}}(\hat{a}'_1 - \hat{a}'_4), \qquad \hat{a}''_4 = \frac{1}{\sqrt{2}}(\hat{a}'_1 + \hat{a}'_4), \quad (61)$$

$$\hat{a}'''_2 = \frac{1}{\sqrt{2}}(\hat{a}''_2 - \hat{a}'_3), \qquad \hat{a}''_3 = \frac{1}{\sqrt{2}}(\hat{a}''_2 + \hat{a}'_3), \quad (62)$$

where $\hat{a}''_2 = \mathrm{e}^{\jmath\pi/2}\hat{a}'_2 = \jmath\hat{a}'_2$. Moreover,

$$\hat{a}''_1 = \frac{1}{2}(\hat{a}_1 - \hat{a}_2 - \hat{a}_3 - \hat{a}_4), \quad (63)$$

$$\hat{a}'''_2 = \frac{1}{2}(-\hat{a}_1 + \jmath\hat{a}_2 - \hat{a}_3 - \jmath\hat{a}_4), \quad (64)$$

$$\hat{a}''_3 = \frac{1}{2}(\hat{a}_1 + \jmath\hat{a}_2 + \hat{a}_3 - \jmath\hat{a}_4), \quad (65)$$

$$\hat{a}''_4 = \frac{1}{2}(\hat{a}_1 + \hat{a}_2 - \hat{a}_3 + \hat{a}_4). \quad (66)$$

Photo currents at photo detectors are defined to be $\hat{I}_1 = \hat{a}''^{\dagger}_1\hat{a}''_1$, $\hat{I}_2 = \hat{a}'''^{\dagger}_2\hat{a}'''_2$, $\hat{I}_3 = \hat{a}''^{\dagger}_3\hat{a}''_3$, and $\hat{I}_4 = \hat{a}''^{\dagger}_4\hat{a}''_4$. The final output currents $\hat{I}_X$ and $\hat{I}_Y$ are

$$\begin{aligned}\hat{I}_X &= \hat{I}_4 - \hat{I}_1 \\ &= \frac{1}{2}\Big(\hat{a}^\dagger_1\hat{a}_2 + \hat{a}^\dagger_2\hat{a}_1 + \hat{a}^\dagger_1\hat{a}_4 + \hat{a}^\dagger_4\hat{a}_1 \\ &\qquad -\hat{a}^\dagger_2\hat{a}_3 - \hat{a}^\dagger_3\hat{a}_2 - \hat{a}^\dagger_3\hat{a}_4 - \hat{a}^\dagger_4\hat{a}_3\Big) \quad (67)\end{aligned}$$

and

$$\begin{aligned}\hat{I}_Y &= \hat{I}_3 - \hat{I}_2 \\ &= \jmath\frac{1}{2}\Big(\hat{a}^\dagger_1\hat{a}_2 - \hat{a}^\dagger_2\hat{a}_1 - \hat{a}^\dagger_1\hat{a}_4 + \hat{a}^\dagger_4\hat{a}_1 \\ &\qquad -\hat{a}^\dagger_2\hat{a}_3 + \hat{a}^\dagger_3\hat{a}_2 - \hat{a}^\dagger_3\hat{a}_4 + \hat{a}^\dagger_4\hat{a}_3\Big). \quad (68)\end{aligned}$$

Further,

$$\begin{aligned}\hat{I}^2_X &= \frac{1}{4}\Big(\hat{a}^{\dagger 2}_1\hat{a}^2_2 + \hat{a}^2_1\hat{a}^{\dagger 2}_2 \\ &\qquad +2\hat{a}^\dagger_1\hat{a}_1 + 2\hat{a}^\dagger_1\hat{a}_1\hat{a}^\dagger_2\hat{a}_2 + 2\hat{a}^\dagger_2\hat{a}_2 + \hat{R}_1\Big) \quad (69)\end{aligned}$$

and

$$\begin{aligned}\hat{I}^2_Y &= -\frac{1}{4}\Big(\hat{a}^{\dagger 2}_1\hat{a}^2_2 + \hat{a}^2_1\hat{a}^{\dagger 2}_2 \\ &\qquad -2\hat{a}^\dagger_1\hat{a}_1 - 2\hat{a}^\dagger_1\hat{a}_1\hat{a}^\dagger_2\hat{a}_2 - 2\hat{a}^\dagger_2\hat{a}_2 + \hat{R}_2\Big), \quad (70)\end{aligned}$$

where the terms $\hat{R}_1$ and $\hat{R}_2$ vanish when the modes $\hat{a}_3$ and $\hat{a}_4$ are in the vacuum state $|0\rangle$.

When the state of port 1 is $|\beta;\mu,\nu\rangle$ and the local oscillator at port 2 is $|A\mathrm{e}^{\jmath\phi}\rangle_{\mathrm{coh}}$ with $A > 0$, then

$$\begin{aligned}\bar{I}_X &= \langle\hat{I}_X\rangle \\ &= A \times \frac{\Lambda_-[\phi]\beta^* + \Lambda^*_-[\phi]\beta}{2}, \quad (71)\end{aligned}$$

$$\begin{aligned}\bar{I}_Y &= \langle\hat{I}_Y\rangle \\ &= A \times \jmath\frac{\Lambda_+[\phi]\beta^* - \Lambda^*_+[\phi]\beta}{2}. \quad (72)\end{aligned}$$

The variances and covariance of I_X and I_Y are

$$\begin{aligned}\Sigma^2_X &= \langle\hat{I}^2_X\rangle - \langle\hat{I}_X\rangle^2 \\ &= A^2 \times \frac{1}{4}\Big(\big|\Lambda_-[\phi]\big|^2 + 1\Big) + \frac{\bar{n}_1}{2} \\ &\approx A^2 \times \frac{1}{4}\Big(\big|\Lambda_-[\phi]\big|^2 + 1\Big), \quad (73)\end{aligned}$$

$$\begin{aligned}\Sigma^2_Y &= \langle\hat{I}^2_Y\rangle - \langle\hat{I}_Y\rangle^2 \\ &= A^2 \times \frac{1}{4}\Big(\big|\Lambda_+[\phi]\big|^2 + 1\Big) + \frac{\bar{n}_1}{2} \\ &\approx A^2 \times \frac{1}{4}\Big(\big|\Lambda_+[\phi]\big|^2 + 1\Big), \quad (74)\end{aligned}$$

$$\begin{aligned}\Sigma_{XY} &= \langle\hat{I}_X\hat{I}_Y\rangle - \langle\hat{I}_X\rangle\langle\hat{I}_Y\rangle \\ &= A^2\Big\{\jmath\frac{1}{8}(\Lambda^*_-[\phi]\Lambda_+[\phi] - \Lambda_-[\phi]\Lambda^*_+[\phi])\Big\}, \quad (75)\end{aligned}$$

where $\bar{n}_1 = |\mu^*\beta - \nu\beta^*|^2 + |\nu|^2$ and where the approximation holds when A is large enough. Re-scaling these statistics by A, $\bar{I}_X \to \bar{X}_{\mathrm{sq}}$, $\bar{I}_Y \to \bar{Y}_{\mathrm{sq}}$, $\Sigma^2_X \to \sigma^2_{X,\mathrm{two,sq}}$, $\Sigma^2_Y \to \sigma^2_{Y,\mathrm{two,sq}}$, and $\Sigma_{XY}/(\Sigma_X\Sigma_Y) \to \zeta_{XY}$.

IV. Detection of BPSK squeezed state signal

Consider a binary phase-shift keying (BPSK) squeezed state signal:

$$|\texttt{signal 0}\rangle = |-\beta;\mu,\nu\rangle, \quad (76)$$

$$|\texttt{signal 1}\rangle = |\beta;\mu,\nu\rangle. \quad (77)$$

Applying the homodyne measurement corresponding to $\{|x\rangle\langle x|\}$, the means of $p(x|\texttt{signal b})$, $\texttt{b} = 0, 1$, are

$$\bar{X}_1 = \frac{\Lambda_-[\phi]\beta^* + \Lambda^*_-[\phi]\beta}{2} = -\bar{X}_0 \quad (78)$$

and the variances are

$$\sigma^2_1 = \frac{1}{4}\big|\Lambda_-[\phi]\big|^2 = \sigma^2_0. \quad (79)$$

The signal-to-noise ratio (SNR) is defined by

$$\mathsf{SNR} = \frac{(\Lambda_-[\phi]\beta^* + \Lambda^*_-[\phi]\beta)^2}{\big|\Lambda_-[\phi]\big|^2}. \quad (80)$$

The average number of signal photons is

$$\bar{N}_0 = |\mu\beta^* - \nu^*\beta|^2 + |\nu|^2 = \bar{N}_1. \quad (81)$$

Suppose $\bar{X}_1 > 0$. Letting $\mathcal{D}_0 = (-\infty, 0)$ be the decision region for $|\texttt{signal 0}\rangle$ and $\mathcal{D}_1 = [0, \infty)$ for $|\texttt{signal 1}\rangle$. The conditional probability of detecting signal 0 (or 1) when signal 1 (or 0) was sent is

$$\begin{aligned}P(0|1) &= \int_{\mathcal{D}_0} p(x|\beta;\mu,\nu)\mathrm{d}x \\ &= \frac{1}{2}\mathsf{erfc}[\frac{\bar{X}_1}{\sigma_1\sqrt{2}}] \\ &= \frac{1}{2}\mathsf{erfc}[\frac{\Lambda_-[\phi]\beta^* + \Lambda^*_-[\phi]\beta}{\sqrt{2\big|\Lambda_-[\phi]\big|^2}}] \\ &= \frac{1}{2}\mathsf{erfc}[\sqrt{\frac{\mathsf{SNR}}{2}}] \\ &= P(1|0) \equiv \epsilon, \quad (82)\end{aligned}$$

where $\mathrm{erfc}[\cdot]$ is the complementary error function.

Since the complementary error function is a monotonically decreasing function, the maximum SNR yields the minimum average probability of error. Therefore, the maximization problem of SNR with respect to (β, μ, ν) is considered under the following constraints:

$$\bar{N}_0 = \bar{N}_1 \le N, \tag{83}$$
$$|\mu|^2 - |\nu|^2 = 1, \tag{84}$$
$$\mu \mathrm{e}^{\jmath\phi} = c\nu \mathrm{e}^{-\jmath\phi}, \quad c > 1, \tag{85}$$

where the third constraint determines the homodyning angle ϕ.

Introducing $\tilde{\mu} = \mu \mathrm{e}^{\jmath\phi}$ and $\tilde{\nu} = \nu \mathrm{e}^{-\jmath\phi}$, the third constraint becomes $\tilde{\mu}/\tilde{\nu} = c > 1$. Hence $|\tilde{\mu}| > |\tilde{\nu}|$ and $\arg(\tilde{\mu}) = \arg(\tilde{\nu})$. As a result, the problem is rewritten as follows:

Maximize

$$\mathsf{SNR} = \frac{(\tilde{\nu}\beta^* + \tilde{\nu}^*\beta)^2}{|\tilde{\nu}|^2}, \tag{86}$$

subject to

$$|\tilde{\mu}\beta^* - \tilde{\nu}^*\beta|^2 + |\tilde{\nu}|^2 \le N, \tag{87}$$
$$|\tilde{\mu}|^2 - |\tilde{\nu}|^2 = 1, \tag{88}$$
$$\tilde{\mu} = c\tilde{\nu}, \quad c > 1. \tag{89}$$

Using the method of Lagrange multipliers, the optimum values of β, $\tilde{\mu}$, and $\tilde{\nu}$ are derived as follows:

$$\beta^\circ = \sqrt{N(N+1)}, \tag{90}$$
$$\tilde{\mu}^\circ = \frac{N+1}{\sqrt{2N+1}}, \tag{91}$$
$$\tilde{\nu}^\circ = \frac{N}{\sqrt{2N+1}}. \tag{92}$$

The SNR of randomly generated parameters is numerically examined for simple verification of the optimality of the parameters above. In the numerical simulation, parameters β, $\tilde{\mu}$, $\tilde{\nu}$ are randomly generated in accordance with the constraint of Eqs. (87)-(89) for given N. The result is shown in Fig. 7, which includes the cases of $N = 10$, 5, and 1 (See also Appendix *B*). In each case, the total number of trials is more than 5000. The graphs indicate that any SNR of randomly generated parameters (blue dot) does not exceed the SNR of the optimal parameters β°, $\tilde{\mu}^\circ$, $\tilde{\nu}^\circ$ (red line).

Therefore, the optimum parameters for the original problem are

$$\beta^\circ = \sqrt{N(N+1)}, \tag{93}$$
$$\mu^\circ = \frac{N+1}{\sqrt{2N+1}} \mathrm{e}^{-\jmath\phi}, \tag{94}$$
$$\nu^\circ = \frac{N}{\sqrt{2N+1}} \mathrm{e}^{\jmath\phi}, \tag{95}$$

and the maximum of the SNR is

$$\mathsf{SNR}^\circ = 4N(N+1). \tag{96}$$

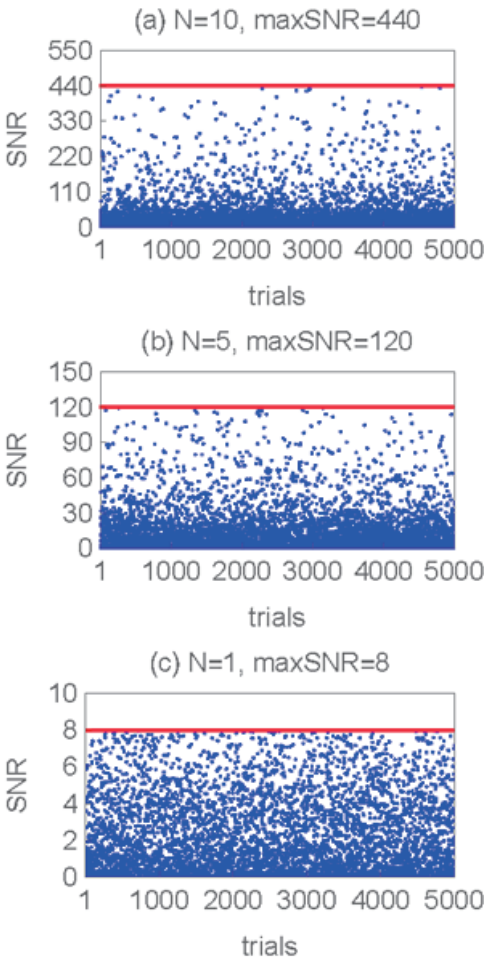

Fig. 7. Optimality of Eqs. (90)-(92).

The means and variances of the PDFs $p(x|\texttt{signal 0})$ and $p(x|\texttt{signal 0})$ are respectively

$$\bar{X}_1^\circ = \sqrt{\frac{N(N+1)}{2N+1}} = -\bar{X}_0^\circ \tag{97}$$

and

$$\sigma_0^{\circ 2} = \frac{1}{4(2N+1)} = \sigma_1^{\circ 2}. \tag{98}$$

Therefore, the average probability of error by the ϕ-rotated homodyne receiver based on the one-component measurement is

$$\begin{aligned} \bar{P}_{\mathrm{e,hom,one}} &= \epsilon \\ &= \frac{1}{2}\mathsf{erfc}[\sqrt{2N(N+1)}] \\ &\approx \frac{1}{2\sqrt{2\pi N(N+1)}} \exp[-2N(N+1)], \end{aligned} \tag{99}$$

for $N \gg 1$.

Here let us consider the case of the two-component measurement type homodyne receiver. For the BPSK squeezed state signal of $|\texttt{signal 0}\rangle = |-\beta^\circ; \mu^\circ, \nu^\circ\rangle$

and $|\texttt{signal 1}\rangle = |\beta^\circ; \mu^\circ, \nu^\circ\rangle$, the PDFs possess the following parameters:

$$\Lambda_-[\phi] = \frac{1}{\sqrt{2N+1}}, \quad \Lambda_+[\phi] = \sqrt{2N+1}, \tag{100}$$

and

$$\bar{X}_1 = \sqrt{\frac{N(N+1)}{2N+1}} = -\bar{X}_0, \tag{101}$$

$$\sigma^2_{X,1} = \frac{N+1}{4N+2} = \sigma^2_{X,0}, \tag{102}$$

$$\bar{Y}_1 = 0 = \bar{Y}_0, \tag{103}$$

$$\sigma^2_{Y,1} = \frac{N+1}{2} = \sigma^2_{Y,0}, \tag{104}$$

$$\zeta_{XY,1} = 0 = \zeta_{XY,0}. \tag{105}$$

Hence,

$$p(x,y|\texttt{signal b}) = \frac{1}{2\pi\sigma_{X,\texttt{b}}\sigma_{Y,\texttt{b}}} \times \exp\Big[-\frac{(x-\bar{X}_\texttt{b})^2}{2\sigma^2_{X,\texttt{b}}} - \frac{y^2}{2\sigma^2_{Y,\texttt{b}}}\Big], \tag{106}$$

for $\texttt{b} = 0, 1$. Fig. 8 shows the graphical images in the standard coordinate $(X_\mathrm{c}, X_\mathrm{s})$ and in the rotated coordinate (X, Y) with angle ϕ. In this figure, the red points stand for the signal 0 and the blue points the signal 1. (See also Appendix *F*).

Letting

$$\mathcal{D}_0 = \{(x,y) : -\infty < x < 0, -\infty < y < \infty\}, \tag{107}$$

$$\mathcal{D}_1 = \{(x,y) : 0 \le x < \infty, -\infty < y < \infty\}, \tag{108}$$

the conditional probabilities of erroneous detection are

$$P(0|1) = \int_{\mathcal{D}_0} p(x,y|\texttt{signal 1})\mathrm{d}x\mathrm{d}y = \frac{1}{2}\mathrm{erfc}[\sqrt{\frac{\gamma}{2}}] = P(1|0) \tag{109}$$

where

$$\gamma = \frac{\bar{X}_1^2}{\sigma^2_{X,1}} = 2N. \tag{110}$$

Hence

$$\bar{P}_{\mathrm{e,hom,two}} = \frac{1}{2}\mathrm{erfc}[\sqrt{N}] \approx \frac{1}{2\sqrt{\pi N}}\exp[-N] \tag{111}$$

Finally, the minimum average probability of error by the optimal quantum receiver, so-called the Helstrom bound, for the BPSK signal of $|\texttt{signal 0}\rangle = |-\beta^\circ; \mu^\circ, \nu^\circ\rangle$ and $|\texttt{signal 1}\rangle = |\beta^\circ; \mu^\circ, \nu^\circ\rangle$ is given by

$$\bar{P}_{\mathrm{e,oqr}} = \frac{1}{2}\Big(1 - \sqrt{1 - \exp[-4N(N+1)]}\Big) \approx \frac{1}{4}\exp[-4N(N+1)] \tag{112}$$

for $N \gg 1$ (See also [3] and Appendix *D*).

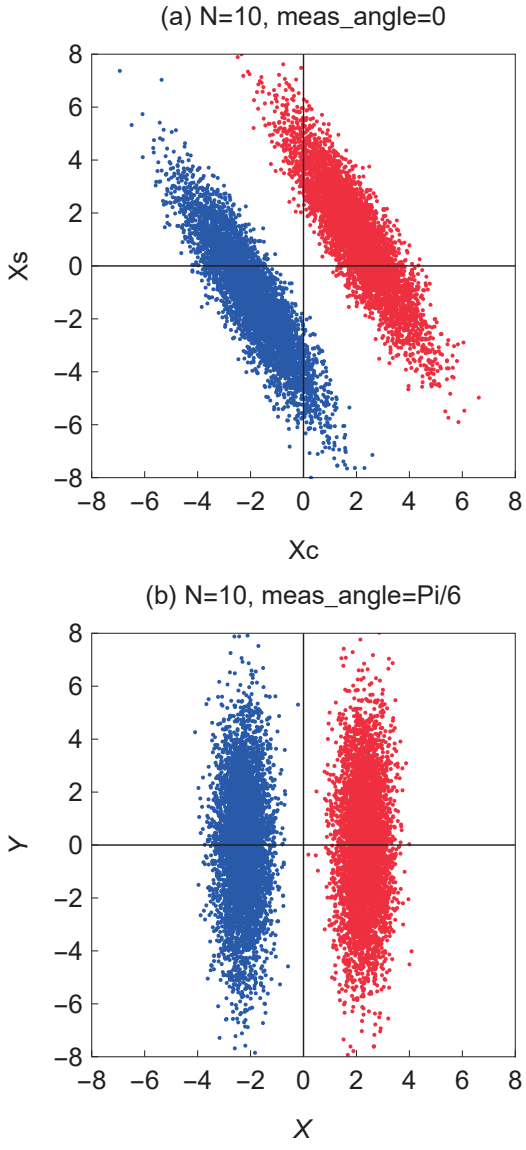

Fig. 8. BPSK signal image in the homodyne detection by two-component measurement. (a) Measurement angle 0 — coordinate $(X_\mathrm{c}, X_\mathrm{s})$. (b) Measurement angle $\phi = \pi/6$ — coordinate (X, Y).

The average probability of error $\bar{P}_{\mathrm{e,hom,one}}$ is plotted in Fig. 9, together with the cases of the optimal quantum receiver, $\bar{P}_{\mathrm{e,oqr}}$, and the two-component measurement homodyne receiver, $\bar{P}_{\mathrm{e,hom,two}}$. In this figure, one can observe that the one-component measurement homodyne receiver follows the optimal quantum receiver keeping almost 1.6 dB degradation in power. However, the two-component measurement homodyne receiver does not behave so.

V. Conclusion

Homodyne measurement with angle ϕ rotation was discussed in the scenario of quantum communications.

First, the probability density functions of measurement outcomes for squeezed states and homodyne measure-

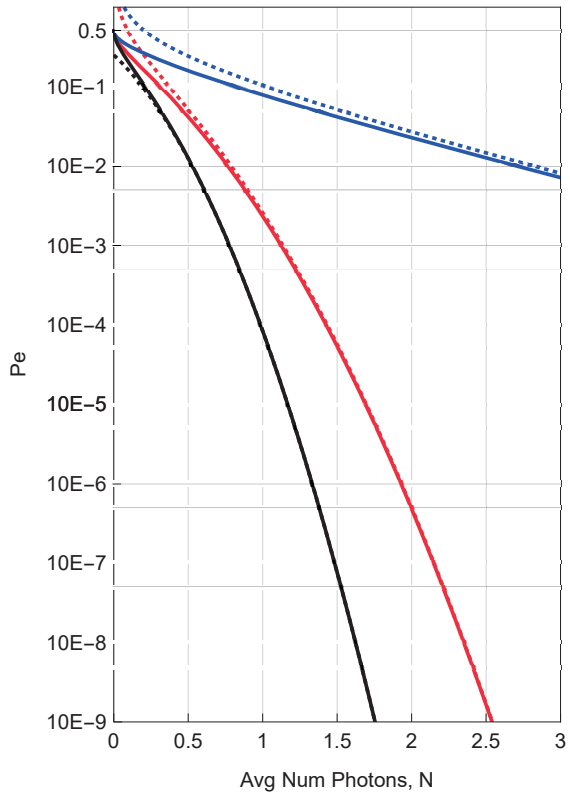

Fig. 9. $P_{\rm e}$ vs. N for BPSK squeezed state signal. $\bar{P}_{\rm e,hom,one}$: solid red line, and its approximation: dotted red line. $\bar{P}_{\rm e,hom,two}$: solid blue line, and its approximation: dotted blue line. $\bar{P}_{\rm e,oqr}$: solid black line, and its approximation: dotted black line.

ment with angle ϕ rotation were derived. The physical implementation schemes corresponding to the rotated homodyne measurements were investigated. Second, the homodyne receiver with angle ϕ rotation was applied to the signal detection problem of the BPSK squeezed state signal. The homodyne receiver of the one-component measurement follows the optimal quantum receiver keeping almost 1.6 dB degradation in power. However, the homodyne receiver of the two-component measurement does not behave so; the required power to achieve the given error probability relatively rises than that of the one-component measurement homodyne in the case of two-component measurement homodyne as the error probability becomes small. This constant degradation property is an advantage of the one-component measurement homodyne receiver against the two-component measurement homodyne. This performance difference may be helpful in cryptographic systems like the quantum stream cipher Y-00 [24], [25]. Detailed analysis and discussions on the application to quantum cryptographic systems will be given elsewhere.

ACKNOWLEDGEMENT

The author is grateful to Prof. Ken Tanizawa of Tamagawa University for his enlightening discussions on the possibility of controlling local oscillators. The idea of the application of homodyne measurement with angle ϕ rotation to quantum communication systems, including cryptographic-purpose receivers, was brought by him.

This material is based upon work supported by the Air Force Office of Scientific Research underaward number FA2386-20-1-4051.

REFERENCES

[1] C. W. Helstrom, QUANTUM DETECTION AND ESTIMATION THEORY (Academic Press, New York, 1976).

[2] H. P. Yuen, and J. Shapiro, "Optical communication with two-photon coherent states – Part I: Quantum-state propagation and quantum-noise reduction," *IEEE Trans. Inf. Theory*, vol.24, iss. 6, pp. 657–668, Nov. 1978.

[3] J. H. Shapiro, H. P. Yuen, and J. A. Machad Mata, "Optical communication with two-photon coherent states —- Part II: Photoemissive detection and structured receiver performance," *IEEE Trans. Inf. Theory*, vol.25, iss. 2, pp. 179–192, Mar. 1979.

[4] H. P. Yuen, and J. H. Shapiro, "Optical communication with two-photon coherent states – Part III: Quantum measurements realizable with photoemissive detectors," *IEEE Trans. Inf. Theory*, vol.26, iss. 1, pp. 78–92, Jan. 1980.

[5] H. P. Yuen and V. W. S. Chan, "Noise in homodyne and heterodyne detection," *Opt. Lett.*, vol. 8, no. 3, pp. 177–179, 1983.

[6] B. L. Schumaker, "Noise in homodyne detection," *Opt. Lett.*, vol. 9, no. 5, pp. 189–191, May 1984.

[7] K. Vogel and H. Risken, "Determination of quasiprobability distributions in terms of probability distribution for rotated quadrature phase," *Phys. Rev. A*, vol. 40, no. 5, pp. 2847–2849, Sep. 1989.

[8] D. T. Smithey, *et al.*, "Measurement of the Wigner distribution and the density matrix of a light mode using optical homodyne tomography: Application to squeezed states and the vacuum," *Phys. Rev. Lett.*, vol. 70, no. 9, pp. 1244–1247, Mar. 1993.

[9] G. M. D'Ariano, C. Macchiavello, and M. G. A. Paris, "Detection of the density matrix through optical homodyne tomography vnthout filtered back projection," *Phys. Rev. A*, vol. 50, no. 5, pp. 4298–4302, Nov. 1994.

[10] A. I. Lvovsky, and M. G. Raymer, "Continuous-variable optical quantum-state tomography," *Rev. Mod. Phys.*, vol. 81, no. 1, pp. 299–331, Jan.-Mar. 2009.

[11] H. P. Yuen, "Two-photon coherent states of the radiation field," *Phys. Rev. A*, vol. 13, no. 6, pp. 2226–2243, 1976.

[12] D.F.Walls, "Squeezed states of light," *Nature*, vol. 306, no. 10, pp. 141–146, Nov. 1983.

[13] O. Hirota, ed., SQUEEZED LIGHT (Elsevier, Amsterdom, 1992); - original ed. in Japanese (Morikita Publishing, Tokyo, 1990).

[14] H. P. Yuen, "Uncertainty principle and the standard quantum limits," arXiv:quant-ph/0510069v1 10 Oct 2005

[15] O. Hirota, S. Ikehara, H. P. Yuen, and R. S. Kennedy, "Generalized coheret state and information content of quantum measurement process," *Paper of Tech. Group on Opt. and Quant. Electron., IECEJ*, OQE75–79, pp. 9–16, Nov. 1975

[16] O. Hirota, "Generalized quantum measurement theory and its application in quantum communication theory (Optical communication by two-photon laser)," *Electron. Commun. Jpn.*, vol. 60, pp. 701–708, 1977.

[17] E. M. F. Curado, *et al.*, "Helstrom bound for squeezed coherent states in binary communication," *Entropy*, vol. 24, no. 2, 220, 2022.

[18] R. Bhadani, and I. B. Djordjevic, "Optimized squeezing operation for phase-shift keying quantum state discrimination," *IEEE Access*, vol. 10, pp. 63383–63393, Jun. 2022.

[19] "Investigation of light wave propagation in atmospheric disturbance toward quantum illumination," *Proc. SPIE*, vol. 11835, 118350E, 2021

[20] G. Masada, "Investigation of propagation characteristics of laser light and squeezed light in fog," *Proc. SPIE*, vol. 12238, 1223804, 2022.

[21] H. P. Robertson, "The uncertainty principle," *Phys. Rev.*, vol. 34, no. 1, pp. 163–164, 1929.

[22] K. Kato, "A note on the error probability by homodyne receiver for M-ary PSK coherent state signal via optical transmission lines with amplifiers," *Tamagawa Univ. Quant. ICT Res. Inst. Bulletin*, vol. 9, no. 1, pp. 33-39, 2019.
[23] H. P. Yuen, "States that give the maximum signal-to-quantum noise ratio for a fixed energy," *Phys. Lett.* vol. 56A, no. 2, pp. 105-106, Mar. 1976.
[24] H. P. Yuen, "KCQ: A new approach to quantum cryptography I. General principles and key generation," arXiv:quant-ph/0311061v6 30 Jul 2004.
[25] M. Sohma, and O. Hirota, "Quantum stream cipher based on Holevo–Yuen theory," *Entropy* vol. 24, no. 5, 667. 2022.
[26] G. E. P. Box and M. E. Muller. "A note on the generation of random normal deviates," *Ann. Math. Statist.* vol. 29, no. 2, pp. 610–611, June, 1958.
[27] D. E. Knuth, THE ART OF COMPUTER PROGRAMMING: VOLUME 2/SEMINUMERICAL ALGORITHMS, 3rd ed. (Addison-Wesley, Boston, 1998).

APPENDIX

A. Squeezed states

This appendix summarizes some basic properties of the squeezed states of light that are used in this article, based on Yuen's formulation [11].

Consider a single mode of the field with photon annihilation operator $\hat{a}$ and creation operator $\hat{a}^\dagger$, and define $\hat{b} = \mu\hat{a} + \nu\hat{a}^\dagger$, where the complex prameters μ and ν satisfy $|\mu|^2 - |\nu|^2 = 1$ (Eqs. (3.1) and (3.2) of [11]). Then $[\hat{b}, \hat{b}^\dagger] = 1$ (Eq. (3.3) of [11]). The squeezed states $|\beta;\mu,\nu\rangle$ are defined to be engenstates of $\hat{b}$, *i.e.*, $\hat{b}|\beta;\mu,\nu\rangle = \beta|\beta;\mu,\nu\rangle$, where $\beta \in \mathbb{C}$ is the eigenvalue of $|\beta;\mu,\nu\rangle$ and $\langle\beta;\mu,\nu|\beta;\mu,\nu\rangle = 1$ (Eq. (3.10) of [11]). The squeezed states are mutually non-orthogonal,

$$\langle\beta';\mu,\nu|\beta;\mu,\nu\rangle = \exp[\beta'^*\beta - \frac{|\beta'|^2}{2} - \frac{|\beta|^2}{2}],$$

and satisfy the overcompleteness relation,

$$\frac{1}{\pi}\int |\beta;\mu,\nu\rangle\langle\beta,\mu,\nu|\mathrm{d}^2\beta = \hat{1}.$$

(Eqs. (3.14) and (3.13) of [11]). From $\hat{b} = \mu\hat{a} + \nu\hat{a}^\dagger$ and $\hat{b}^\dagger = \mu^*\hat{a}^\dagger + \nu^*\hat{a}$, $\hat{a} = \mu^*\hat{b} - \nu\hat{b}^\dagger$ and $\hat{a}^\dagger = \mu\hat{b}^\dagger - \nu^*\hat{b}$ (Eq. (3.27) of [11]). Therefore,

$$\begin{aligned}
\langle\hat{a}\rangle &= \langle\beta;\mu,\nu|\hat{a}|\beta;\mu,\nu\rangle = \mu^*\beta - \nu\beta^*,\\
\langle\hat{a}^\dagger\rangle &= \mu\beta^* - \nu^*\beta,\\
\langle\hat{a}^2\rangle &= (\mu^*\beta - \nu\beta^*)^2 - \mu^*\nu,\\
\langle\hat{a}^{\dagger 2}\rangle &= (\mu\beta^* - \nu^*\beta)^2 - \mu\nu^*,\\
\langle\hat{a}^\dagger\hat{a}\rangle &= |\mu^*\beta - \nu\beta^*|^2 + |\nu|^2,\\
\langle(\Delta\hat{a})^2\rangle &= \langle(\hat{a} - \langle\hat{a}\rangle)^2\rangle = -\mu^*\nu,\\
\langle(\Delta\hat{a})^{\dagger 2}\rangle &= -\mu\nu^*,\\
\langle(\Delta\hat{a})^\dagger(\Delta\hat{a})\rangle &= |\nu|^2
\end{aligned}$$

(Eqs. (3.28) and (3.29) of [11]).

Let $\hat{a} \equiv \hat{X}_\mathrm{c} + \jmath\hat{X}_\mathrm{s}$, $\hat{X}_\mathrm{c} = \hat{X}_\mathrm{c}^\dagger$ and $\hat{X}_\mathrm{s} = \hat{X}_\mathrm{s}^\dagger$ (Eq. (2.5) of [11]). Hence $\hat{X}_\mathrm{c} = (\hat{a}^\dagger + \hat{a})/2$, $\hat{X}_\mathrm{s} = \jmath(\hat{a}^\dagger - \hat{a})/2$, and $[\hat{X}_\mathrm{c}, \hat{X}_\mathrm{s}] = \jmath/2$ (Eq. (3.33) of [11]). For $\hat{X}_\mathrm{c}$ and $\hat{X}_\mathrm{s}$,

$$\begin{aligned}
\langle\hat{X}_\mathrm{c}\rangle &= \frac{(\mu-\nu)\beta^* + (\mu^*-\nu^*)\beta}{2}\\
\langle\hat{X}_\mathrm{s}\rangle &= \jmath\frac{(\mu+\nu)\beta^* - (\mu^*+\nu^*)\beta}{2}\\
\langle(\Delta\hat{X}_\mathrm{c})^2\rangle &= \frac{1}{4}|\mu-\nu|^2\\
\langle(\Delta\hat{X}_\mathrm{s})^2\rangle &= \frac{1}{4}|\mu+\nu|^2\\
\langle(\Delta\hat{X}_\mathrm{c})(\Delta\hat{X}_\mathrm{s})\rangle &= \jmath\frac{1}{4}(\mu^*\nu - \mu\nu^* + 1)\\
\langle(\Delta\hat{X}_\mathrm{s})(\Delta\hat{X}_\mathrm{c})\rangle &= \jmath\frac{1}{4}(\mu^*\nu - \mu\nu^* - 1)
\end{aligned}$$

(Eqs. (3.28) and (3.29) of [11]).

Define the eigenstates $|x_\mathrm{c}\rangle$ by $\hat{X}_\mathrm{c}|x_\mathrm{c}\rangle = x_\mathrm{c}|x_\mathrm{c}\rangle$ and $\langle x_\mathrm{c}|x_\mathrm{c}\rangle = 1$. Then the collection $\{|x_\mathrm{c}\rangle\langle x_\mathrm{c}| : x_\mathrm{c} \in \mathbb{R}\}$ is a projection-valued measure. The x_c-representation of $|\beta;\mu,\nu\rangle$ is

$$\begin{aligned}
\langle x_\mathrm{c}|\beta;\mu,\nu\rangle &= \left(\frac{2}{\pi}\right)^{1/4}\left(\frac{1}{\mu-\nu}\right)^{1/2}\\
&\quad\times\exp[-\frac{\mu+\nu}{\mu-\nu}x_\mathrm{c}^2 + \frac{2}{\mu-\nu}\beta x_\mathrm{c}\\
&\quad -\frac{1}{2}|\beta|^2 - \frac{1}{2}\cdot\frac{(\mu-\nu)^*}{\mu-\nu}\beta^2]
\end{aligned}$$

(Eq. (3.24) of [11]). Therefore, the probability density function of measurement outcome x_c by $\{|x_\mathrm{c}\rangle\langle x_\mathrm{c}|\}$ is

$$\begin{aligned}
&p(x_\mathrm{c}|\beta,\mu,\nu)\\
&\quad= \big|\langle x_\mathrm{c}|\beta;\mu,\nu\rangle\big|^2\\
&\quad= \sqrt{\frac{2}{\pi|\mu-\nu|^2}}\exp\big[-\frac{2}{|\mu-\nu|^2}\\
&\qquad\times\left(x_\mathrm{c} - \frac{(\mu-\nu)\beta^* + (\mu^*-\nu^*)\beta}{2}\right)^2\big].
\end{aligned}$$

Recall that the coherent states $|\alpha\rangle_\mathrm{coh}$ form a positive operator-valued measure, $\{|\alpha\rangle_\mathrm{coh}\langle\alpha|/\pi : \alpha \in \mathbb{C}\}$. The wave function by the coherent state $|\alpha\rangle_\mathrm{coh}$ is

$$\begin{aligned}
&{}_\mathrm{coh}\langle\alpha|\beta;\mu,\nu\rangle\\
&\quad= \frac{1}{\sqrt{\mu}}\exp\Big[-\frac{1}{2}|\alpha|^2 - \frac{1}{2}|\beta|^2\\
&\qquad -\frac{\nu}{2\mu}\alpha^{*2} + \frac{\nu^*}{2\mu}\beta^2 + \frac{1}{\mu}\alpha^*\beta\Big] \qquad (113)
\end{aligned}$$

(Eq. (3.20) of [11]). Therefore, the probability density function of measurement outcome $\alpha = x_\mathrm{c} + \jmath x_\mathrm{s}$ by

$\{|\alpha\rangle_{\rm coh}\langle\alpha|/\pi\}$ is

$$
\begin{aligned}
&p(x_{\rm c},x_{\rm s}|\beta;\mu,\nu)\\
&\quad= \frac{1}{\pi}|{}_{\rm coh}\langle\alpha|\beta;\mu,\nu\rangle|^2\\
&\quad= \frac{1}{\pi|\mu|}\exp\Big[-(1-2C_1)(x_{\rm c}-\bar{X}_{\rm c,sq})^2\\
&\qquad\qquad -(1+2C_1)(x_{\rm s}-\bar{X}_{\rm s,sq})^2\\
&\qquad\qquad +4C_2(x_{\rm c}-\bar{X}_{\rm c,sq})(x_{\rm s}-\bar{X}_{\rm s,sq})\Big]
\end{aligned}
$$

where $x_{\rm c}=(\alpha^*+\alpha)/2$, $x_{\rm s}=\jmath(\alpha^*-\alpha)/2$,

$$
\begin{aligned}
\bar{X}_{\rm c,sq} &= \frac{(\mu-\nu)\beta^*+(\mu^*-\nu^*)\beta}{2},\\
\bar{X}_{\rm s,sq} &= \jmath\frac{(\mu+\nu)\beta^*-(\mu^*+\nu^*)\beta}{2},\\
C &= -\frac{\nu}{2\mu}\equiv C_1+\jmath C_2,\\
C_1 &= -\frac{1}{4|\mu|^2}(\mu^*\nu+\mu\nu^*),\\
C_2 &= \jmath\frac{1}{4|\mu|^2}(\mu^*\nu-\mu\nu^*).
\end{aligned}
$$

(Eq. (3.38) of [11]). This can be written in the standard Gaussian form,

$$
\begin{aligned}
&p(x_{\rm c},x_{\rm s}|\beta;\mu,\nu)\\
&\quad= \frac{1}{2\pi\sigma_{\rm c,two,sq}\sigma_{\rm s,two,sq}\sqrt{1-\zeta_{\rm cs}^2}}\\
&\qquad\times\exp\Big[-\frac{1}{2(1-\zeta_{\rm cs}^2)}\\
&\qquad\quad\times\Big\{\frac{(x_{\rm c}-\bar{X}_{\rm c,sq})^2}{\sigma_{\rm c,two,sq}^2}+\frac{(x_{\rm s}-\bar{X}_{\rm s,sq})^2}{\sigma_{\rm s,two,sq}^2}\\
&\qquad\quad -2\zeta_{\rm cs}\frac{(x_{\rm c}-\bar{X}_{\rm c,sq})(x_{\rm s}-\bar{X}_{\rm s,sq})}{\sigma_{\rm c,two,sq}\sigma_{\rm s,two,sq}}\Big\}\Big], \quad (114)
\end{aligned}
$$

where

$$
\begin{aligned}
\sigma_{\rm c,two,sq}^2 &= \frac{1+2C_1}{2(1-4|C|^2)}=\frac{1}{4}\Big(|\mu-\nu|^2+1\Big),\\
\sigma_{\rm s,two,sq}^2 &= \frac{1-2C_1}{2(1-4|C|^2)}=\frac{1}{4}\Big(|\mu+\nu|^2+1\Big),\\
\zeta_{\rm cs} &= \frac{2C_2}{\sqrt{1-4C_1^2}}\\
&= \jmath\frac{\mu^*\nu-\mu\nu^*}{\sqrt{(|\mu-\nu|^2+1)(|\mu+\nu|^2+1)}},
\end{aligned}
$$

and in the following form by the covariant matrix $\mathbf{K}$,

$$
\begin{aligned}
&p(x_{\rm c},x_{\rm s}|\beta;\mu,\nu)\\
&\quad= \frac{1}{2\pi\sqrt{\det(\mathbf{K}_{\rm cs})}}\\
&\qquad\times\exp[-\frac{1}{2}(\mathbf{x}_{\rm cs}-\mathbf{m}_{\rm cs})^t\mathbf{K}_{\rm cs}^{-1}(\mathbf{x}_{\rm cs}-\mathbf{m}_{\rm cs})],
\end{aligned}
$$

where $\mathbf{x}_{\rm cs}=[x_{\rm c},x_{\rm s}]^t$, $\mathbf{m}_{\rm cs}=[\bar{X}_{\rm c},\bar{X}_{\rm s}]^t$,

$$
\begin{aligned}
&\mathbf{x}_{\rm cs}=\begin{bmatrix}x_{\rm c}\\ x_{\rm s}\end{bmatrix},\quad \mathbf{m}_{\rm cs}=\begin{bmatrix}\bar{X}_{\rm c}\\ \bar{X}_{\rm s}\end{bmatrix}\\
&\mathbf{K}_{\rm cs}=\frac{1}{4}\begin{bmatrix}|\mu-\nu|^2+1 & \jmath(\mu^*\nu-\mu\nu^*)\\ \jmath(\mu^*\nu-\mu\nu^*) & |\mu+\nu|^2+1\end{bmatrix},\\
&\det(\mathbf{K}_{\rm cs})=\frac{1}{4}|\mu|^2,\\
&\mathbf{K}_{\rm cs}^{-1}=\frac{1}{|\mu|^2}\begin{bmatrix}|\mu+\nu|^2+1 & -\jmath(\mu^*\nu-\mu\nu^*)\\ -\jmath(\mu^*\nu-\mu\nu^*) & |\mu-\nu|^2+1\end{bmatrix}
\end{aligned}
$$

(Eq. (3.43) of [11]).

In terms of the complex measurement outcomes (α^*,α), the probability density function $p(x_{\rm c},x_{\rm s}|\beta,\mu,\nu)$ can be rewritten as

$$
\begin{aligned}
&p(\alpha^*,\alpha|\beta;\mu,\nu)\\
&\quad=\frac{1}{2\pi\sqrt{\det(\mathbf{K}_{\rm amp})}}\\
&\qquad\times\exp[-\frac{1}{2}(\mathbf{x}_{\rm amp}-\mathbf{m}_{\rm amp})^\dagger\mathbf{K}_{\rm amp}^{-1}(\mathbf{x}_{\rm amp}-\mathbf{m}_{\rm amp})],
\end{aligned}
$$

where

$$
\begin{aligned}
&\mathbf{x}_{\rm amp}=\mathbf{\Omega}_{\rm cs}^{\rm amp}\mathbf{x}_{\rm cs}=\frac{1}{\sqrt{2}}\begin{bmatrix}\alpha\\ \alpha^*\end{bmatrix},\\
&\mathbf{m}_{\rm amp}=\mathbf{\Omega}_{\rm cs}^{\rm amp}\mathbf{m}_{\rm cs}=\frac{1}{\sqrt{2}}\begin{bmatrix}\bar{X}_{\rm c}+\jmath\bar{X}_{\rm s}\\ \bar{X}_{\rm c}-\jmath\bar{X}_{\rm s}\end{bmatrix},\\
&\qquad=\frac{1}{\sqrt{2}}\begin{bmatrix}-\nu\beta^*+\mu^*\beta\\ \mu\beta^*-\nu^*\beta\end{bmatrix},\\
&\mathbf{K}_{\rm amp}=\mathbf{\Omega}_{\rm cs}^{\rm amp}\mathbf{K}_{\rm cs}(\mathbf{\Omega}_{\rm cs}^{\rm amp})^{-1}\\
&\qquad=\frac{1}{4}\begin{bmatrix}|\mu|^2+|\nu|^2+1 & -2\mu^*\nu\\ -2\mu\nu^* & |\mu|^2+|\nu|^2+1\end{bmatrix},\\
&\det(\mathbf{K}_{\rm amp})=\frac{1}{4}|\mu|^2,\\
&\mathbf{K}_{\rm amp}^{-1}\\
&\qquad=\frac{1}{|\mu|^2}\begin{bmatrix}|\mu|^2+|\nu|^2+1 & 2\mu^*\nu\\ 2\mu\nu^* & |\mu|^2+|\nu|^2+1\end{bmatrix},
\end{aligned}
$$

and

$$
\begin{aligned}
\mathbf{\Omega}_{\rm cs}^{\rm amp} &= \frac{1}{\sqrt{2}}\begin{bmatrix}1 & \jmath\\ 1 & -\jmath\end{bmatrix},\\
(\mathbf{\Omega}_{\rm cs}^{\rm amp})^{-1} &= \frac{1}{\sqrt{2}}\begin{bmatrix}1 & 1\\ -\jmath & \jmath\end{bmatrix}=(\mathbf{\Omega}_{\rm cs}^{\rm amp})^\dagger
\end{aligned}
$$

(Eq. (3.49) of [11]).

The Weyl characteristic function is

$$
\begin{aligned}
&\chi_{\rm w}(\xi_1,\xi_2)\\
&\quad= \langle\beta;\mu,\nu|{\rm e}^{\xi\hat{a}^\dagger-\xi^*\hat{a}}|\beta;\mu,\nu\rangle\\
&\quad= \exp\Big[-\frac{1}{2}|\mu+\nu|^2\xi_1^2-\frac{1}{2}|\mu-\nu|^2\xi_2^2\\
&\qquad +\jmath(\mu^*\nu-\mu\nu^*)\xi_1\xi_2\\
&\qquad +\big\{(\mu+\nu)\beta^*-(\mu^*+\nu^*)\beta\big\}\xi_1\\
&\qquad +\jmath\big\{(\mu-\nu)\beta^*+(\mu^*-\nu^*)\beta\big\}\xi_2\Big]\\
&\quad= \exp[\jmath\boldsymbol{\xi}_{\rm cs}^t\mathbf{m}_{\rm cs}-\frac{1}{2}\boldsymbol{\xi}_{\rm cs}^t\tilde{\mathbf{K}}_{\rm cs}\boldsymbol{\xi}_{\rm cs}],
\end{aligned}
$$

where

$$\boldsymbol{\xi}_{\rm cs} = \left[\begin{array}{c} 2\xi_2 \\ -2\xi_1 \end{array} \right], \quad \xi = \xi_1 + \jmath\xi_2,$$
$$\tilde{\mathbf{K}}_{\rm cs} = \frac{1}{4}\left[\begin{array}{cc} |\mu-\nu|^2 & \jmath(\mu^*\nu - \mu * \nu^*) \\ \jmath(\mu^*\nu - \mu * \nu^*) & |\mu+\nu|^2 \end{array} \right].$$

In terms of the complex parameters (ξ^*, ξ), it becomes

$$\chi_{\rm w}(\xi^*,\xi) = \exp[\jmath\boldsymbol{\xi}_{\rm cpx}^\dagger \mathbf{m}_{\rm cpx} - \frac{1}{2}\boldsymbol{\xi}_{\rm cpx}^\dagger \tilde{\mathbf{K}}_{\rm cpx}\boldsymbol{\xi}_{\rm cpx}],$$

where

$$\begin{aligned}
\boldsymbol{\xi}_{\rm cpx} &= \boldsymbol{\Omega}_{\rm cs}^{\rm cpx}\boldsymbol{\xi}_{\rm cs} = \sqrt{2}\left[\begin{array}{c} \xi \\ \xi^* \end{array} \right], \\
\mathbf{m}_{\rm cpx} &= \boldsymbol{\Omega}_{\rm cs}^{\rm cpx}\mathbf{m}_{\rm cs} = \jmath\frac{1}{\sqrt{2}}\left[\begin{array}{c} \bar{X}_{\rm c} + \jmath\bar{X}_{\rm s} \\ -\bar{X}_{\rm c} + \jmath\bar{X}_{\rm s} \end{array} \right] \\
&= \jmath\frac{1}{\sqrt{2}}\left[\begin{array}{c} -\nu\beta^* + \mu^*\beta \\ -\mu\beta^* + \nu^*\beta \end{array} \right], \\
\tilde{\mathbf{K}}_{\rm cpx} &= \boldsymbol{\Omega}_{\rm cs}^{\rm cpx}\tilde{\mathbf{K}}_{\rm cs}(\boldsymbol{\Omega}_{\rm cs}^{\rm cpx})^{-1} \\
&= \frac{1}{4}\left[\begin{array}{cc} |\mu|^2+|\nu|^2 & 2\mu^*\nu \\ 2\mu\nu^* & |\mu|^2+|\nu|^2 \end{array} \right],
\end{aligned}$$

and

$$\boldsymbol{\Omega}_{\rm cs}^{\rm cpx} = \frac{1}{\sqrt{2}}\left[\begin{array}{cc} \jmath & -1 \\ -\jmath & -1 \end{array} \right].$$

The Wigner function is given by

$$\begin{aligned}
&W(x_{\rm c}, x_{\rm s}) \\
&= \frac{1}{\pi^2}\int \chi_{\rm w}(\xi^*,\xi)\mathrm{e}^{\xi^*\alpha - \xi\alpha^*}\mathrm{d}^2\xi \\
&= \frac{2}{\pi}\exp\Big[-2|\mu+\nu|^2x_{\rm c}^2 - 2|\mu-\nu|^2x_{\rm s}^2 \\
&\qquad +4\jmath(\mu^*\nu - \mu\nu^*)x_{\rm c}x_{\rm s} \\
&\qquad +2\big\{(\mu+\nu)\beta^* + (\mu^*+\nu^*)\beta\big\}x_{\rm c} \\
&\qquad +2\jmath\big\{(\mu-\nu)\beta^* - (\mu^*-\nu^*)\beta\big\}x_{\rm s} \\
&\qquad -2|\beta|^2\Big],
\end{aligned}$$

which satisfies

$$\begin{aligned}
p(x_{\rm c}|\beta,\mu,\nu) &= \int_{-\infty}^{\infty} W(x_{\rm c}, x_{\rm s})\mathrm{d}x_{\rm s} \\
p(x_{\rm s}|\beta,\mu,\nu) &= \int_{-\infty}^{\infty} W(x_{\rm c}, x_{\rm s})\mathrm{d}x_{\rm c}
\end{aligned}$$

B. Some example data in Fig. 7

(Small SNR case) For $N = 10$,

$$\begin{aligned}
\beta &= -0.036791 + 0.53594\jmath, \\
\tilde{\mu} &= 1.96644 + 1.60260\jmath, \\
\tilde{\nu} &= 1.80720 + 1.47283\jmath
\end{aligned}$$

were generated in a trial. These parameters numerically satisfy the conditions $|\tilde{\mu}\beta^* + \tilde{\nu}^*\beta|^2 + |\tilde{\nu}|^2 = N$, $|\tilde{\mu}|^2 - |\tilde{\nu}|^2 = 1$, and $\tilde{\mu}/\tilde{\nu} = 1.08811 > 1$. Then $\mathsf{SNR} = 0.384549 \ll \mathsf{SNR}^\circ = 440$.

(Moderate SNR case) For $N = 5$,

$$\begin{aligned}
\beta &= 3.84034 + 0.029892\jmath, \\
\tilde{\mu} &= 2.14668 + 0.112682\jmath, \\
\tilde{\nu} &= 1.90025 + 0.099747\jmath, \\
\tilde{\mu}/\tilde{\nu} &= 1.12968 > 1,
\end{aligned}$$

and $\mathsf{SNR} = 58.8787 < \mathsf{SNR}^\circ = 120$.

(Large SNR case) For $N = 1$,

$$\begin{aligned}
\beta &= -1.07011 - 0.889929\jmath, \\
\tilde{\mu} &= -0.867301 - 0.690319\jmath, \\
\tilde{\nu} &= -0.374213 - 0.297851\jmath, \\
\tilde{\mu}/\tilde{\nu} &= 2.31767 > 1,
\end{aligned}$$

and $\mathsf{SNR} = 7.74489 \lesssim \mathsf{SNR}^\circ = 8$.

C. Wingner function in (X, Y)

In the coordinate X, Y, the Wigner function of $|\beta;\mu,\nu\rangle$ is calculated as

$$\begin{aligned}
&W(x,y) \\
&= \frac{2}{\pi}\int_{-\infty}^{\infty}\langle x+x'|\beta;\mu,\nu\rangle\langle\beta;\mu,\nu|x-x'\rangle\mathrm{e}^{-4\jmath yx'}\mathrm{d}x' \\
&= \frac{2}{\pi}\exp[-2\big|\Lambda_+[\phi]\big|^2x^2 - 2\big|\Lambda_-[\phi]\big|^2y^2 \\
&\qquad +2\jmath\big(\Lambda_-^*[\phi]\Lambda_+[\phi] - \Lambda_-[\phi]\Lambda_+^*[\phi]\big)xy \\
&\qquad +2\big(\Lambda_+[\phi]\beta^* + \Lambda_+^*[\phi]\beta\big)x \\
&\qquad +2\jmath\big(\Lambda_-[\phi]\beta^* - \Lambda_-^*[\phi]\beta\big)y - 2|\beta|^2]. \qquad (115)
\end{aligned}$$

This provides

$$\begin{aligned}
p(x|\beta;\mu,\nu) &= \int_{-\infty}^{\infty} W(x,y)\mathrm{d}y, \qquad (116) \\
p(y|\beta;\mu,\nu) &= \int_{-\infty}^{\infty} W(x,y)\mathrm{d}x. \qquad (117)
\end{aligned}$$

Further, the matrix representation of $|\beta;\mu,\nu\rangle$ is

$$\begin{aligned}
&\langle x+x'|\beta;\mu,\nu\rangle\langle\beta;\mu,\nu|x-x'\rangle \\
&\qquad = \int_{-\infty}^{\infty} W(x,y)\mathrm{e}^{4\jmath yx'}\mathrm{d}y, \qquad (118) \\
&\langle y+y'|\beta;\mu,\nu\rangle\langle\beta;\mu,\nu|y-y'\rangle \\
&\qquad = \int_{-\infty}^{\infty} W(x,y)\mathrm{e}^{-4\jmath y'x}\mathrm{d}x. \qquad (119)
\end{aligned}$$

D. Helstrom bound

For binary phase-shift keying (BPSK) squeezed state signal,

$$\begin{aligned}
|\texttt{signal 0}\rangle &= |-\beta;\mu,\nu\rangle, \qquad (120) \\
|\texttt{signal 1}\rangle &= |\beta;\mu,\nu\rangle, \qquad (121)
\end{aligned}$$

the minimum of the average probability of error by the optimal quantum receiver, so-called the Helstrom bound, is given by

$$\bar{P}_{\rm e}^{\rm quant}(\beta;\mu,\nu) = \frac{1}{2}\left(1 - \sqrt{1-\exp[-4|\beta|^2]}\right). \qquad (122)$$

Then the minimization of $\bar{P}_{\rm e}^{\rm quant}(\beta;\mu,\nu)$ with constraint

$$|\mu\beta^* - \nu^*\beta|^2 + |\nu|^2 \leq N \tag{123}$$

for given N determines the optimal values of the parameters [3] (See also [23]):

$$\beta^\circ = \sqrt{N(N+1)}, \tag{124}$$

$$\mu^\circ = \frac{N+1}{\sqrt{2N+1}}, \tag{125}$$

$$\nu^\circ = \frac{N}{\sqrt{2N+1}}. \tag{126}$$

Hence

$$\bar{P}_{\rm e}^{\rm quant}(\beta^\circ;\mu^\circ,\nu^\circ) = \frac{1}{2}\left(1-\sqrt{1-\exp[-4N(N-1)]}\right). \tag{127}$$

E. Some properties of Λ_- and Λ_+

$$\Lambda_-^*[\phi]\Lambda_+[\phi] + \Lambda_-[\phi]\Lambda_+^*[\phi] = 2,$$

$$\Lambda_-^*[\phi]\Lambda_+[\phi] - \Lambda_-[\phi]\Lambda_+^*[\phi] = 2(\mu^*\nu {\rm e}^{-2\jmath\phi} - \mu\nu^* {\rm e}^{2\jmath\phi}),$$

$$\Lambda_-[\phi+\frac{\pi}{2}] = \jmath\Lambda_+[\phi],$$

$$\Lambda_+[\phi+\frac{\pi}{2}] = \jmath\Lambda_-[\phi].$$

F. Numerical simulation method for PDF

Suppose U_1 and U_2 are independent random variables uniformly distributed on the interval $(0,1)$. If

$$V_1 = \sqrt{-2\ln U_1}\cos(2\pi U_2), \tag{128}$$

$$V_2 = \sqrt{-2\ln U_1}\sin(2\pi U_2), \tag{129}$$

then V_1 and V_2 obeys the normal distribution $\mathcal{N}(0,1)$. This generation method is called Box-Muller method [26].

Suppose V_1 and V_2 are independent normal random variables with mean 0 and variance 1. If

$$W_1 = \bar{W}_1 + \sigma_1 V_1, \tag{130}$$

$$W_2 = \bar{W}_2 + \sigma_2(\zeta V_1 + \sqrt{1-\zeta^2}V_2), \tag{131}$$

then W_1 and W_2 are dependent random variables, distributed as two-dimensional normal distribution with means $\bar{W}_1$,$\bar{W}_2$, variances σ_1^2, σ_2^2, and correlation coefficient ζ [27].